



**Formation of Box Canyon, Idaho, by Megaflood:
Implications for Seepage Erosion on Earth and Mars**
Michael P. Lamb, *et al.*
Science **320**, 1067 (2008);
DOI: 10.1126/science.1156630

**The following resources related to this article are available online at
www.sciencemag.org (this information is current as of May 25, 2008):**

Updated information and services, including high-resolution figures, can be found in the online version of this article at:

<http://www.sciencemag.org/cgi/content/full/320/5879/1067>

Supporting Online Material can be found at:

<http://www.sciencemag.org/cgi/content/full/320/5879/1067/DC1>

This article **cites 23 articles**, 3 of which can be accessed for free:

<http://www.sciencemag.org/cgi/content/full/320/5879/1067#otherarticles>

This article appears in the following **subject collections**:

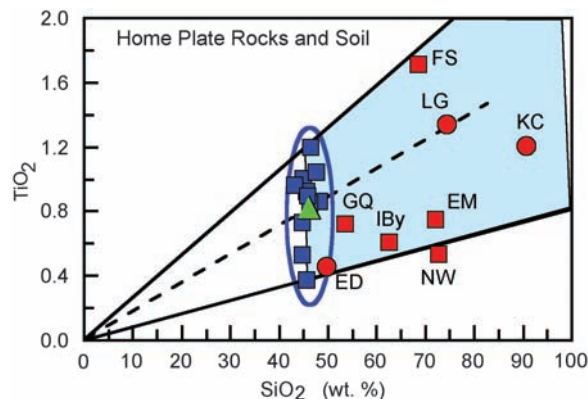
Planetary Science

http://www.sciencemag.org/cgi/collection/planet_sci

Information about obtaining **reprints** of this article or about obtaining **permission to reproduce this article** in whole or in part can be found at:

<http://www.sciencemag.org/about/permissions.dtl>

Fig. 5. Plot of titanium dioxide and silica contents for APXS measurements acquired since arriving at Home Plate and including observations from the Eastern Valley, Low Ridge, Mitchelltree Ridge, and the Tyrone areas. Red squares, silica-rich rocks; red circles, silica-rich soils; blue squares, basaltic rocks in the vicinity of Home Plate; and green triangle, typical local soil. The light blue region represents the compositions that can be obtained by acid-sulfate leaching of Home Plate rocks, assuming no variation in the $\text{TiO}_2/\text{SiO}_2$ ratio. KC, Kenosha Comets; LG, Lefty Ganote; FS, Fuzzy Smith; EM, Elizabeth Mahon; NW, Nancy Warren; ED, Eileen Dean; Iby, Innocent Bystander; and GQ, Good Question. The dashed line represents a typical evolutionary trend for leaching that preserves SiO_2 and TiO_2 , and the blue oval indicates the range of basaltic rock compositions in the vicinity of Home Plate.



25. P. M. Dove, J. D. Rimstidt, in *Silica: Physical Behavior, Geochemistry and Materials Applications*, P. J. Heaney, C. T. Prewitt, G. V. Gibbs, Eds. (Mineralogical Society of America, Washington, DC, vol. 29, 1994) pp. 259–308.
26. R. V. Morris *et al.*, *Lunar Planet. Sci.* **XXXI**, 2014 (2000).
27. K. A. Rodgers *et al.*, *Earth Sci. Rev.* **66**, 1 (2004).
28. K. A. Rodgers *et al.*, *Clay Miner.* **37**, 299 (2002).
29. H. D. Nam *et al.*, *Jpn. J. Appl. Phys.* **37**, 4603 (1998).
30. S. J. Kim, S. D. Park, Y. H. Jeong, *J. Am. Ceram. Soc.* **82**, 927 (1999).
31. W. P. Inskeep, T. R. McDermott, *Geothermal Biology and Geochemistry in Yellowstone National Park* (Thermal Biology Institute, Bozeman, MT, 2003).
32. M. R. Walter, D. J. Des Marais, *Icarus* **101**, 129 (1993).
33. W. N. Doemel, T. D. Brock, *Appl. Environ. Microbiol.* **34**, 433 (1977).
34. P. L. Siering *et al.*, *Geomicrobiol. J.* **23**, 129 (2006).
35. S. L. Cady, J. D. Farmer, in *Evolution of Hydrothermal Ecosystems on Earth (and Mars?)*, G. Bock, J. Goode, Eds. (J. Wiley and Sons, Chichester, UK, 1996), pp. 150–173.
36. S. Murchie *et al.*, *J. Geophys. Res.* **112**, E05503 (2007).
37. R. E. Milliken *et al.*, Abstract P12A-02, presented at the American Geophysical Union Fall Meeting, San Francisco, CA, 10 to 14 December 2007.
38. This research was carried out for the Jet Propulsion Laboratory, California Institute of Technology, under a contract with NASA.

Supporting Online Material

www.sciencemag.org/cgi/content/full/320/5879/1063/DC1
Figs. S1 to S4
Table S1

18 January 2008; accepted 15 April 2008
10.1126/science.1155429

- and dragged this nonrotating wheel along the surface, scraping paths through soils and crushing weak rocks.
17. J. W. Salisbury *et al.*, *Infrared (2.1–25 μm) Spectra of Minerals* (Johns Hopkins Univ. Press, Baltimore, 1991).
 18. J. W. Salisbury *et al.*, *J. Geophys. Res.* **92**, 702 (1987).
 19. J. F. Bell III *et al.*, *J. Geophys. Res.* **108**, 8063 (2003).
 20. M. S. Rice *et al.*, Abstract #2138, presented at the 39th Annual Lunar and Planetary Science Conference, Houston, TX, 10 to 14 March 2008.

21. K. E. Herkenhoff *et al.*, *J. Geophys. Res.* **108**, 8065 (2003).
22. G. Klingelhöfer *et al.*, *J. Geophys. Res.* **108**, 8067 (2003).
23. Most of the rock and soil targets on the east side of Home Plate are named after players and teams from the All American Girls Professional Baseball League that operated from 1943 to 1954. The names are informal and not approved by the International Astronomical Union.
24. R. E. Arvidson *et al.*, *J. Geophys. Res.* **111**, E02501 (2006).

Formation of Box Canyon, Idaho, by Megaflood: Implications for Seepage Erosion on Earth and Mars

Michael P. Lamb,* William E. Dietrich, Sarah M. Aciego, Donald J. DePaolo, Michael Manga

Amphitheater-headed canyons have been used as diagnostic indicators of erosion by groundwater seepage, which has important implications for landscape evolution on Earth and astrobiology on Mars. Of perhaps any canyon studied, Box Canyon, Idaho, most strongly meets the proposed morphologic criteria for groundwater sapping because it is incised into a basaltic plain with no drainage network upstream, and approximately 10 cubic meters per second of seepage emanates from its vertical headwall. However, sediment transport constraints, ^4He and ^{14}C dates, plunge pools, and scoured rock indicate that a megaflood (greater than 220 cubic meters per second) carved the canyon about 45,000 years ago. These results add to a growing recognition of Quaternary catastrophic flooding in the American northwest, and may imply that similar features on Mars also formed by floods rather than seepage erosion.

A central thrust in geomorphology and planetary science is to link diagnostic landscape morphologies to formation processes. A prominent example is the formation of amphitheater-headed canyons, in which the stubby appearance of valley heads, steep headwalls, and little landscape dissection upstream have long been interpreted to result from seepage erosion or groundwater sapping on Earth (1–4), Mars (5, 6), and now Titan (7). Theory (8), ex-

periments (9), and field studies (10) have validated this hypothesis in unconsolidated sand, showing that valley heads are undermined and propagate upstream from seepage-induced erosion. This means that valleys can grow without precipitation-fed overland flow, which has profound implications for landscape evolution on Earth and the hydrologic cycle and habitability of Mars.

Despite widespread acceptance of the seepage-erosion hypothesis and its validation in sand, we lack an unambiguous example of an amphitheater-headed canyon formed by seepage erosion in bedrock because of overlapping features generated by rainfall runoff at most sites on Earth (11).

Even the amphitheater-headed valleys of the Colorado Plateau and Hawaii, which are most often cited as classic examples of groundwater sapping in bedrock (2, 3), have been in question because of evidence for flash floods and plunge-pool erosion (11–13). To better evaluate the seepage-erosion hypothesis, we set out to study the erosion and transport processes within a bedrock canyon, Box Canyon, Idaho, USA, which has a steep amphitheater-shaped headwall, contains the 11th-largest spring in the United States, and lacks the landscape dissection and rainfall runoff upstream of its headwall that has made other sites controversial (Fig. 1A). Moreover, Box Canyon exhibits remarkable similarity in morphology and possibly lithology (basalt) with many Martian canyons (Fig. 1B) that have been attributed to seepage erosion (5, 6).

Box Canyon is located within the Snake River Plain, a broad and relatively flat basin in southern Idaho filled by sediments and volcanic flows that erupted over the course of ~15 million to 2 thousand years ago (ka) (14). Several tributaries of the Snake River Canyon appear as stubby valleys that end abruptly in amphitheater heads, including Malad Gorge, Blind Canyon, and Box Canyon (Fig. 2), all of which have been attributed to seepage erosion (1, 4). Box Canyon is cut into the Sand Springs Basalt [also named the Basalt of Rocky Butte (15); see supporting online material (SOM) text] with an Ar-Ar eruption age of 95 ± 10 ka (16) and U-Th/He eruption ages that range from 86 ± 12 ka to 130 ± 12 ka (17), and this basalt filled an ancestral canyon of the Snake River (18).

Department of Earth and Planetary Science, University of California, Berkeley, CA 94720–4768, USA.

*To whom correspondence should be addressed. E-mail: mpl@berkeley.edu

The permeable lava beds of the Snake River Plain form an extensive aquifer, with recharge entering in the east [for example, Big Lost River sinks (Fig. 2)] and groundwater flowing westward. Large springs emanate from the east wall of the Snake River Canyon between Box Canyon and Malad Gorge, where the river jogs north, perpendicular to the regional topographic slope and the groundwater flow direction. These springs have a cumulative discharge of $\sim 170 \text{ m}^3/\text{s}$, and one of the largest [$\sim 10 \text{ m}^3/\text{s}$ (fig. S6)] emanates from the head of Box Canyon, creating Box Canyon Creek (19).

Box Canyon is sinuous (Fig. 3A), and the longitudinal profile is approximately 2.68 km in length and has an average channel-bed slope of 2.18% (Fig. 3B and fig. S3). The canyon is $\sim 35 \text{ m}$ deep and 120 m wide at its head and about twice as deep and wide at its mouth. The columnar basalt walls of the canyon have collapsed, creating steep ($\sim 20^\circ$ to 35°) talus slopes, many of which abut Box Canyon Creek. Talus accumulation lessens upstream and is absent at the canyon head (Fig. 4A). Several terracelike platforms are elevated 2 to 7 m above the current stream level and separate the steep talus slopes from the creek (Fig. 3 and fig. S3). These contain large boulders ($>1 \text{ m}$), and some appear to be imbricated in the downstream direction, indicating past fluvial transport.

Although the lack of talus at the canyon head has been taken as evidence of continued dissolution (4), the bedrock composing the headwall and surrounding talus are blocky and hard and show no visual evidence for enhanced weathering. Water samples from Box Canyon Creek and neighboring wells have silica concentrations of 32 to 35 mg/l, which bracket the saturation value (see SOM text and fig. S6), suggesting that the groundwater is in equilibrium with the basaltic aquifer and that substantial dissolution is not occurring at Box Canyon spring.

Despite no modern overland flow contribution to Box Canyon Creek, three features at the canyon head indicate that surface water once flowed into the canyon. First, three concentric semicircles of boulders within the canyon head appear to be waterfall plunge pools with $\sim 2 \text{ m}$ of relief (Fig. 4A). Second, a small notch ($\sim 300 \text{ m}^3$) in the center of the headwall rim (Fig. 4A) has linear flutelike abrasion marks, millimeters in width and several centimeters long, that follow the local curvature of the notch, indicating past overspill. The scours appear as divots on the inferred upstream end that gradually fan outward and diminish in relief downstream (Fig. 4B). Third, this scoured rock extends at least 1 km upstream of the canyon head and delineates flow toward the canyon (Fig. 3). The scoured path cannot be followed further upstream because it is covered by loess, deposited from ~ 40 to 10 ka (20).

The basalt in Box Canyon breaks down into large boulders ($\sim 1 \text{ m}$) that, without dissolution, must be transported downstream to allow canyon growth. Despite the great discharge of the spring,

no measurable amount of sediment is currently transported. A minimum estimate of flow needed to carve the canyon can be found by calculating the discharge necessary to initiate sediment

transport on the creek bed. We measured channel cross sections (fig. S4), longitudinal channel-bed profiles (Fig. 3 and fig. S3), and grain-diameter distributions (fig. S2) [diameter (D_{84}) = 0.6 m,

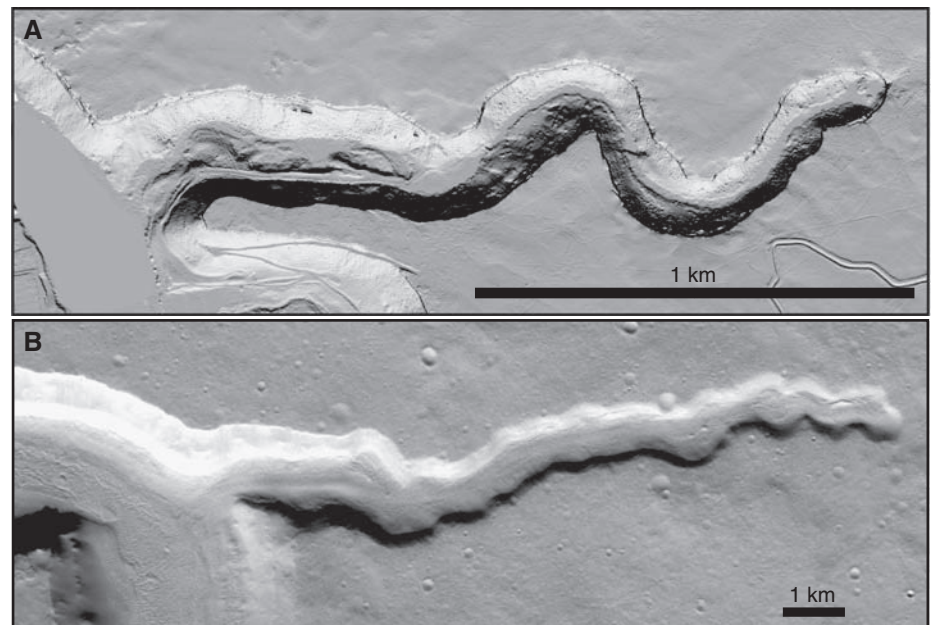


Fig. 1. (A) Shaded relief map of Box Canyon, Idaho. Airborne laser-swath mapping data were collected by the National Center for Airborne Laser Mapping. The data have been filtered to remove vegetation that exists along the creek banks. This is a Universal Transverse Mercator (UTM) zone 11 projection, North American Datum of 1983 (NAD83) datum, at 1 m resolution. (B) Thermal Emission Imaging System (TIS) infrared daytime image of Marners Vallis, Mars, image V19470014, at 19 m resolution.

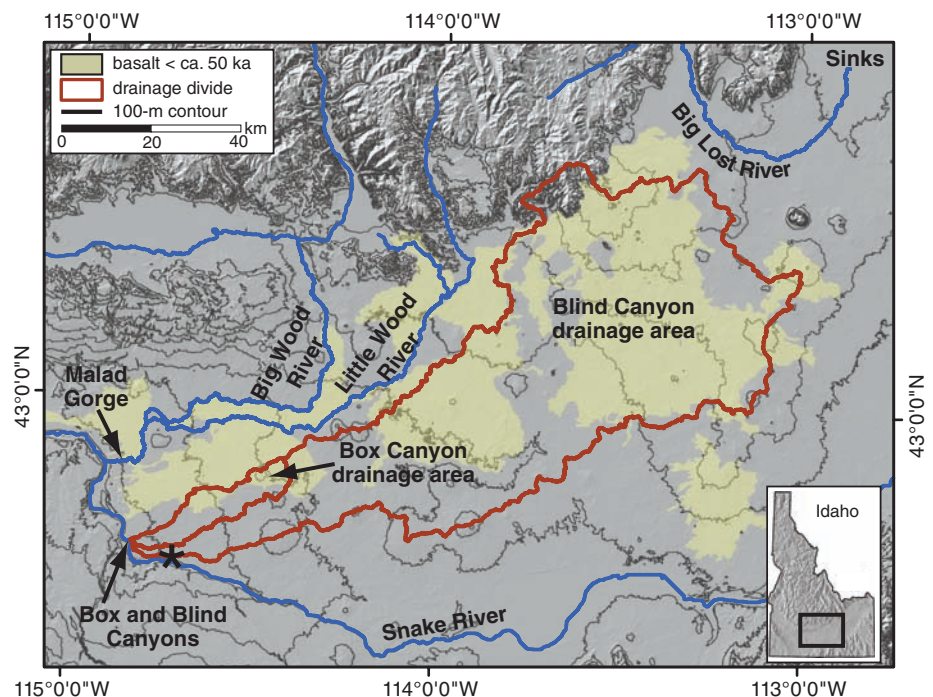


Fig. 2. Topographic map of the eastern Snake River Plain, the location of which is shown on the inset map of Idaho. The drainage areas feeding Box Canyon (228 km^2) and Blind Canyon (4713 km^2) are outlined, following the path of steepest descent. The yellow-shaded regions mark the locations of volcanism younger than $\sim 50 \text{ ka}$ (15). The thin black lines are 100-m topographic contours. Topographic data are from the U.S. Geological Survey. This is a UTM zone 11 projection, NAD83 datum, at 25 m resolution.

$D_{50} = 0.29$ m, and $D_{16} = 0.13$ m; the subscripts denote the percentage of grains that are finer] at a relatively straight 125-m reach within the canyon (Fig. 3A). A critical Shields stress formula for incipient motion (21) combined with our measured channel cross section (XS2 in Fig. 3A and fig. S4), local average bed slope ($S = 1.85\%$; Fig. 3B and fig. S3), and a flow-resistance equation (22) determined that a flow discharge $Q > 220$ m³/s (corresponding to an average flow depth $h > 1.7$ m) would be necessary to move the sediment bed and continue canyon erosion (23). This is a factor of 22 greater than the modern spring discharge ($Q \sim 10$ m³/s).

The scoured-rock upslope of the canyon head occurs within a broad channel-like depression ~ 250 m wide and 3 m deep (XS1 in Fig. 3A and fig. S4). The scours extend over the southern bank of XS1, indicating that flow was deeper than and only partially bounded by this channel. A discharge estimate can be made for the flood event that spilled over the canyon rim by assuming that the flow was contained within this channel. Using the measured cross-sectional area at the threshold of overspill at XS1 (475 m²), the regional bedrock slope parallel to scour marks ($S = 0.74\%$), a flow-resistance formula (22), and a wide range in of bed-roughness length scales

$0.1 \leq k_s \leq 1$ m (because this is the least-constrained parameter), we calculated a minimum flow discharge ranging from 800 to 2800 m³/s (23). This would have filled the canyon to a depth of 3.7 to 5.8 m within our measurement reach (fig. S4), and, unlike seepage, would have exceeded the competency threshold to transport the bouldery bed. These estimated discharges are large, but smaller than the peak discharge of other catastrophic floods in the region [for example, the Bonneville flood, 10^6 m³/s (24), and the Big Lost River Flood, 6×10^4 m³/s (25)].

The vertical profile of the headwall suggests that it migrated upstream as a knickpoint, and the near-vertical joints inherent to flood basalt probably promoted toppling of basalt columns. The lack of gravel upstream of the canyon head also limited abrasion of the canyon rim. If sediment transport was the rate-limiting step for canyon erosion, a duration of flow needed to carve the canyon can be estimated by dividing the total volume of the canyon ($\sim 1.53 \times 10^7$ m³) by a volumetric transport rate of sediment (26) for our estimates of flood discharge (800 to 2800 m³/s). This suggests that flow was sustained for 35 to 160 days to transport the required load out of the canyon (23), which is similar to the estimated duration of the Bonneville flood [~ 100 days (24)]. Excavation of Box Canyon could have taken less time, however, because the flood was only partially contained within the channel at XS1.

We collected four samples, distributed in the streamwise direction within the canyon (Fig. 3), for ³He cosmogenic-exposure-age dating to further constrain the history of the canyon. We sampled scoured bedrock that was exposed at the canyon-head rim [location 4 (Fig. 4B)], and three large boulders that, from their size and separation from the active talus slopes, appeared to be relatively stable (fig. S1B). Active talus production from canyon walls, as well as weathering, means that the ages for these boulder surfaces provide minimum ages of the canyon.

Of the boulders sampled, only location 2 was on a terrace among other large imbricated boulders, potentially indicating past fluvial transport (Fig. 3 and fig. S1B). This sample yielded an exposure age of 48 ± 3 ka (1 σ error) and the other two boulders were nearly half as old

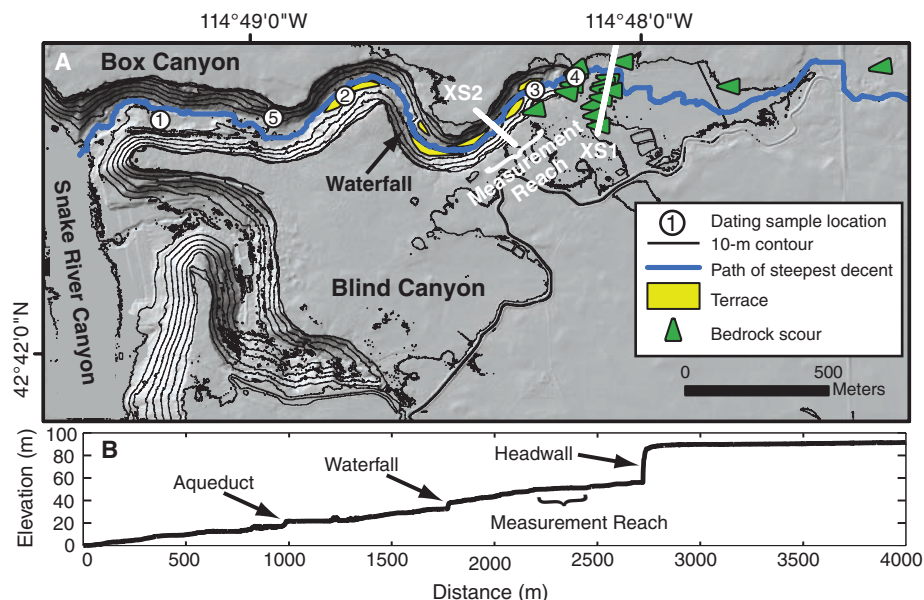


Fig. 3. (A) High-resolution topographic map of Box and Blind Canyons. The yellow-shaded regions mark potential fluvial terraces, which range from 2 to 7 m above the current stream level (fig. S3). Detailed measurements of flow depth, water surface slope, bed slope, channel width, and bed particle size were made within the region marked “measurement reach” (23). Discharge calculations were made using cross-sectional areas measured at XS1 and XS2 (fig. S4). Mapped scours on bedrock (Fig. 4B) are shown as green arrows. The white circles are sample locations used for dating. The thin black lines are 10-m topographic contours. The blue line is the calculated path of steepest descent, but does not indicate modern-day flow paths because no flow on record has spilled over the canyon headwall. See Fig. 1 for data source and projection. (B) Longitudinal profile of Box Canyon extracted from light detection and ranging data (Fig. 3A), following the path of steepest descent. Major breaks in slope correspond to the canyon headwall, waterfall, and a disturbed region near the canyon mouth caused by an aqueduct.

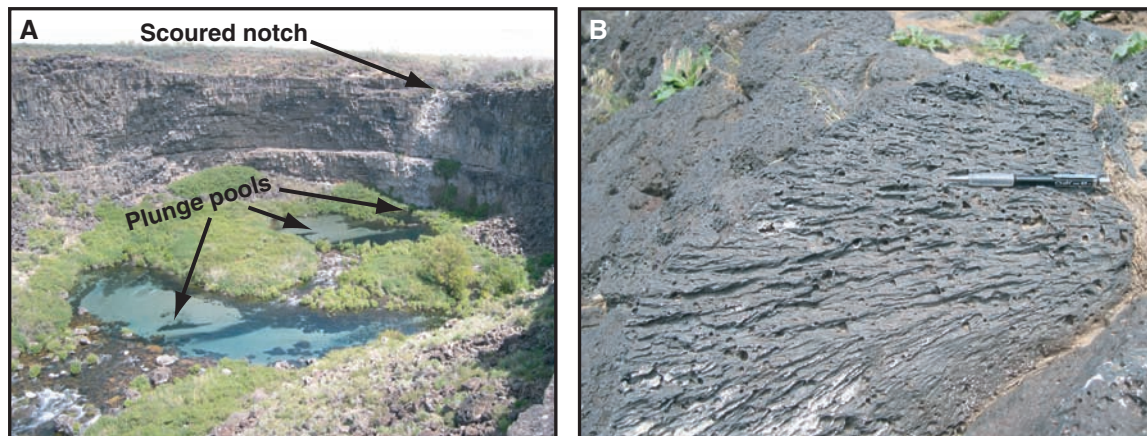


Fig. 4. (A) Photograph of the head of Box Canyon. The three concentric circles that lack boulders are interpreted to be plunge pools. The headwall relief is ~ 35 m. (B) Photograph of scours within the notch of the Box Canyon headwall. The pencil included for scale is ~ 14 cm long and points in the inferred flow direction.

Downloaded from www.sciencemag.org on May 25, 2008

(location 1, 21 ± 1 ka; location 3, 19 ± 3 ka) (17, 23). The scoured notch (location 4) yielded the same age as the boulder at location 2, 45 ± 5 ka.

Another constraint on the age of the canyon comes from an ~20-cm-thick, finely laminated bed, containing clay, silt, and sand, that is exposed in a small road cut within the talus slope [location 5 (Fig. 3 and fig. S1C)]. Two shells found within the layer yielded ages of $22.4 \pm 1 \times 10^3$ radiocarbon years before the present (23), which is equivalent to a calibrated age of ~26 ka (27).

Together, these observations, hydraulic calculations, and dates eliminate the seepage-erosion hypothesis for the formation of Box Canyon. Here, seepage is not substantially enhancing the weathering of the headwall, and contemporary seepage flow is deficient by a factor of ~22 to evacuate sediment from the canyon. Moreover, erosion of the canyon headwall ceased ~45 ka according to the age of the scoured-bedrock notch. The observations of scoured bedrock and plunge pools point toward a flood or floods able to transport boulders and carve the canyon in weeks or months, illustrating the power of rare catastrophic events in shaping landscape. This hypothesis is supported by the similarity in surface-exposure ages of the terrace-bound boulder at location 2 and the scoured notch. We interpret the younger boulders to have rolled to the canyon floor after the canyon was formed, which is consistent with the shell deposit sandwiched between several meters of talus (fig. S1C), indicating that canyon formation occurred well before 22 ka and wall collapse has been active since. Whereas a single flood event is the simplest interpretation, we cannot rule out multiple events occurring after 86 ± 12 ka [the eruption age of the basalt (17)], with the last event resetting the exposure ages to ~45 ka.

The dates indicate that the canyon is much older than the Bonneville flood that occurred within the Snake River Canyon ~14.5 ka. Given the drainage area of Box Canyon (228 km²) and Blind Canyon (4713 km²) (Fig. 2), and our flood-duration and discharge estimates, a sufficient meteorological flood would require more than 1.7 m of runoff lasting for several weeks or longer, which is highly unlikely because modern annual precipitation averages only 0.22 m over the eastern Snake River Plain, infiltration is extremely high, and conditions were probably drier ~45 ka (28). Potential diversions of the Snake River by lava flows also seem unlikely because the Snake River Canyon and the Box and Blind drainages are separated topographically, except for one location (marked with an asterisk on Fig. 2), and no volcanic dams with an age of ~45 ka have been discovered there.

The most likely source for the Box Canyon flood is the Little and Big Wood River drainage basins to the north or the Big Lost River drainage basin to the northeast (Fig. 2). Both drainages produced large-magnitude paleofloods that cut canyons in Quaternary basalt, scoured bedrock, and transported large (~1 m) boulders (15, 25).

For example, the paleomegaflood of the Big Lost River, which occurred sometime between ~19 ka and 95 ka (29), was probably an outburst from the Pleistocene Glacial-Lake East Fork and had a peak flow of 6×10^4 m³/s (25). Such an event would have easily surpassed the drainage divide between Box Canyon and the Wood and Lost River drainages (Fig. 1). The divides themselves also have shifted since the formation of Box Canyon because of volcanism that postdates the Box Canyon flood (Fig. 2).

Our findings suggest that Box Canyon and other amphitheater-headed canyons carved into basalt by large floods [for example, Dry Falls, Washington, USA (30), and Ásbyrgi Canyon, Iceland (31)] might be better terrestrial analogs of Martian canyons in volcanic terrains than seepage channels in sand.

References and Notes

1. I. C. Russel, *U.S. Geol. Surv. Bull.* **199**, 192 (1902).
2. J. E. Laity, M. C. Malin, *Geol. Soc. Am. Bull.* **96**, 203 (1985).
3. R. C. Kocheil, J. F. Piper, *J. Geophys. Res.* **91**, E175 (1986).
4. H. T. Stearns, *J. Geol.* **44**, 429 (1936).
5. M. C. Malin, M. H. Carr, *Nature* **397**, 589 (1999).
6. K. P. Harrison, R. E. Grimm, *J. Geophys. Res.* **10.1029/2001E002455** (2005).
7. M. G. Tomasko et al., *Nature* **438**, 10.1038/nature04126 (2005).
8. T. Dunne, *Prog. Phys. Geogr.* **4**, 211 (1980).
9. A. D. Howard, C. F. McLane, *Water Resour. Res.* **24**, 1659 (1988).
10. S. A. Schumm, K. F. Boyd, C. G. Wolff, W. J. Spitz, *Geomorphology* **12**, 281 (1995).
11. M. P. Lamb et al., *J. Geophys. Res.* **111**, 10.1029/2005JE002663 (2006).
12. M. P. Lamb, A. D. Howard, W. E. Dietrich, J. T. Perron, *Geol. Soc. Am. Bull.* **119**, 805 10.1130/B25986.1 (2007).
13. A. D. Howard, W. E. Dietrich, M. A. Seidl, *J. Geophys. Res.* **99**, 13971 (1994).
14. H. E. Malde, in *Quaternary Nonglacial Geology; Conterminous U.S.*, R. B. Morrison, ed. [Geological Society of America (GSA), Boulder, CO, 1991], vol. K-2.
15. J. D. Kauffman, K. L. Otherberg, V. S. Gillerman, D. L. Garwood, *Geologic Map of the Twin Falls 30 × 60 minute Quadrangle, Idaho* (Idaho Geological Survey, Moscow, ID, 2005).
16. L. Tauxe, C. Luskin, P. Selkin, P. Gans, A. Calvert, *Geochim. Geophys. Geosyst.* **5**, 10.1029/2003GC000661 (2004).
17. S. M. Aciego et al., *Earth Planet. Sci. Lett.* **254**, 288 10.1016/j.epsl.2006.11.039 (2007).
18. H. E. Malde, *U.S. Geol. Surv. Prof. Pap.* **20**, 20 (1971).
19. U.S. Geological Survey: Box Canyon creek, gauge 13095500. This well log information can be found at <http://waterdata.usgs.gov/awis>.
20. S. L. Forman, R. P. Smith, W. R. Hackett, J. A. Tullis, P. A. McDaniel, *Quat. Res.* **40**, 30 (1993).
21. M. P. Lamb, W. E. Dietrich, J. Venditti, *J. Geophys. Res.*, doi:10.1029/2007JF000831 (2008).
22. J. C. Bathurst, *J. Hydrol. (Amst.)* **269**, 11 (2002).
23. Materials and methods are available as supporting material on Science Online
24. J. E. O'Connor, *Hydrology, Hydraulics and Geomorphology of the Bonneville Flood*, (GSA Special Paper 274, GSA, Boulder, CO, 1993), p. 90.
25. S. L. Rathburn, *Geomorphology* **8**, 305 (1993).
26. R. Fernandez Luque, R. van Beek, *J. Hydraul. Res.* **14**, 127 (1976).
27. P. J. Reimer et al., *Radiocarbon* **46**, 1029 (2004).
28. D. B. Madsen et al., *Palaeogeogr. Palaeoclimatol. Palaeoecol.* **167**, 243 (2001).
29. T. E. Cerling, R. J. Poreda, S. L. Rathburn, *Geology* **22**, 227 (1994).
30. J. H. Bretz, *J. Geol.* **31**, 617 (1923).
31. H. Tomasson, *Natururfraeinginnirinn* **43**, 12 (1973).
32. P. R. Christensen et al., *Space Sci. Rev.* **110**, 85 (2004).
33. Funding was provided by the NASA Astrobiology Institute and the National Center for Earth Surface Dynamics. We thank C. May, J. McKean, T. Perron, R. Thurov, and T. van Soest for field assistance.

Supporting Online Material

www.sciencemag.org/cgi/content/full/320/5879/1067/DC1
Materials and Methods
SOM Text
Figs. S1 to S6
Table S1

19 February 2008; accepted 21 April 2008
10.1126/science.1156630

Anticorrelated Seismic Velocity Anomalies from Post-Perovskite in the Lowermost Mantle

Alexander R. Hutko,^{1*} Thorne Lay,^{1†} Justin Revenaugh,² Edward J. Garnero³

Earth's lowermost mantle has thermal, chemical, and mineralogical complexities that require precise seismological characterization. Stacking, migration, and modeling of over 10,000 *P* and *S* waves that traverse the deep mantle under the Cocos plate resolve structures above the core-mantle boundary. A small $-0.07 \pm 0.15\%$ decrease of *P* wave velocity (V_p) is accompanied by a $1.5 \pm 0.5\%$ increase in *S* wave velocity (V_s) near a depth of 2570 km. Bulk-sound velocity [$V_b = (V_p^2 - 4/3V_s^2)^{1/2}$] decreases by $-1.0 \pm 0.5\%$ at this depth. Transition of the primary lower-mantle mineral, $(\text{Mg}_{1-x-y}\text{Fe}_x\text{Al}_y)(\text{Si,Al})\text{O}_3$ perovskite, to denser post-perovskite is expected to have a negligible effect on the bulk modulus while increasing the shear modulus by ~6%, resulting in local anticorrelation of V_b and V_s anomalies; this behavior explains the data well.

Increasing pressure (*P*) and temperature (*T*) with depth in Earth causes minerals to undergo phase transitions to new crystalline structures accompanied by abrupt changes in

density (ρ), isentropic bulk modulus (K_S), and shear modulus (*G*) that result in seismic *P* wave velocity $\{V_p = [(K_S + 4/3G)/\rho]^{1/2}\}$ and *S* wave velocity $[V_s = (G/\rho)^{1/2}]$ discontinuities. The pri-



Supporting Online Material for

Formation of Box Canyon, Idaho, by Megaflood: Implications for Seepage Erosion on Earth and Mars

Michael P. Lamb,* William E. Dietrich, Sarah M. Aciego, Donald J. DePaolo, Michael Manga

*To whom correspondence should be addressed. E-mail: mpl@berkeley.edu

Published 23 May 2008, *Science* **320**, 1067 (2008)
DOI: 10.1126/science.1156630

This PDF file includes:

Materials and Methods
SOM Text
Figs. S1 to S6
Tables S1
References

Supporting Online Materials for:

Formation of Box Canyon Idaho by Megaflood: Implications for Seepage Erosion on Earth and Mars

Michael P. Lamb*, William E. Dietrich, Sarah M. Aciego, Donald J. DePaolo, Michael Manga

*University of California, Department of Earth and Planetary Science
Berkeley, CA, 94720-4768*

*mpl@berkeley.edu

This PDF file includes:

Materials and Methods

SOM Text

Figs. S1 to S6

Table S1

References and Notes

Materials and Methods

Discharge at incipient motion

We estimated the flow needed to carve Box Canyon from the dimensionless bed-shear stress or Shields stress at incipient sediment motion τ_{*c} :

$$\tau_{*c} = \frac{\tau_b}{(\rho_s - \rho)gD_{50}} \quad (1)$$

where τ_b is the bed shear-stress, ρ_s and ρ are the densities of sediment and fluid,

respectively, g is the acceleration due to gravity, and D_{50} is the median grain diameter

($S1$, $S2$). We assume steady and uniform flow, i.e. $\tau_b = \rho g R S$, where R is the hydraulic radius and S is the water-surface slope.

To evaluate equation (1), we made measurements within a 125-m reach (Fig. S1A) along the canyon floor (marked “Measurement Reach” in Fig. 3), which was chosen because it was relatively straight in planform and wadeable. The bed is bouldery throughout the canyon and is probably best described as plane-bed morphology ($S3$), although there are local clusters of boulders and pools. The grain size distribution was measured within this reach (Fig. S2) and the particle-size statistics are $D_{84} = 0.60$ m, $D_{50} = 0.29$ m, and $D_{16} = 0.13$ m, where the subscripts denote the percentage of grains finer than. We measured the intermediate axes of 100 grains by counting particles every 1 m along the channel and conducting four transects spaced ~ 10 m apart (Fig. S1A). Owing to the large size of particles, measurements were made *in situ* using a tape measure and snorkel gear. A few grains were larger than 1 m across and these were counted twice in the distribution. The particle sizes were binned following the phi scale.

The longitudinal profile of the water surface was measured from 1-m resolution airborne Light Detection and Ranging (LiDAR) data collected by the National Center for Airborne Laser Mapping (Fig. S3). The profile was extracted from a digital elevation model (DEM) following the path of steepest descent, and this profile was verified to be accurate by comparison with a field survey within the measurement reach conducted with a self-leveling level and stadia rod. During floods, bed irregularities will be drowned out and the water surface-slope will tend to be more uniform over a length scale of many times the channel width. To account for this, we estimated the water-surface slope during flood as the average water-surface slope over a 900-m reach bounded by the waterfall

downstream and the canyon headwall upstream (Profile P2, Fig. S3). Using a linear least-squares fit, the slope was found to be $S = 1.85\%$, and for this channel slope $\tau_{*c} = 0.055$ (S4). Using these values, the necessary bed shear-stress to move the bouldery bed was calculated from equation (1) to be 290 N/m^2 assuming $(\rho_s - \rho) = 1800 \text{ kg/m}^3$ for basalt.

From these calculations and measurements, the discharge needed to move sediment within the canyon can be calculated from the empirical formula of Bathurst (S5):

$$Q = UA = a(gRS)^{1/2} \left(\frac{h}{k_s} \right)^b A, \quad (2)$$

where U is the average flow velocity across a channel cross section, A is the cross sectional area of flow, h is the average flow depth, and k_s is the roughness length scale of the bed. a and b were found empirically from measurements in mountain streams to be $a = 3.84$ and $b = 0.547$ for $S < 0.8\%$, and $a = 3.1$ and $b = 0.93$ for $S > 0.8\%$ (S5).

Bathurst (S5) suggested $k_s \approx D_{84}$, although this likely depends on the site-specific substrate (e.g., bed forms, particle-size distribution, particle angularity). Others have shown that k_s can be two or three times D_{84} (e.g., S6). Instead of assuming k_s , we calculated it from equation (2) for conditions in Box Canyon creek using our surveyed cross section, water surface profile, and the USGS measured discharge ($Q = 9.15 \text{ m}^3/\text{s}$) from March 2004 (S7). A cross section (XS2, Fig. 3) within the measurement reach was surveyed using a self leveling level and stadia rod (Fig. S4A). At the time of the

measurements, the maximum flow depth was 1.08 m and the average depth over the cross section was $h = 0.58$ m, which is equivalent to a hydraulic radius of $R = 0.57$ m. Within the measurement reach, the water surface slope at the time of our measurements was approximately uniform and equal to 0.9% (Profile P3, Fig. S3). Inserting these values into equation (2) results in $k_s = 0.81$ m, which is about one-third larger than our measured D_{84} within the reach. In the following calculations we use $k_s = 0.81$ m rather than D_{84} making our discharge estimates conservative.

At incipient motion, the hydraulic radius was calculated from equation (1) to be $R = 1.6$ m. Such a flow would fill the canyon at XS2 to an average depth of $h = 1.7$ m and a maximum depth of 2.5 m (Fig. S4A). Using these values and $S = 1.85\%$, equation (2) was solved to find that a discharge $Q > 220$ m³/s is needed to begin to move the sediment bed and continue canyon erosion.

Discharge of the flood event

The scoured channel upstream of the canyon head was used to estimate the discharge of the flood event. Aside from scour marks and a few plucked blocks along bedding planes, most of the bedrock surface within the channel is continuous with the neighboring land surface and appears to be the original volcanic surface. This suggests that the broad channel was not created by the flood event, but rather was inherited topography that likely focused flow towards the canyon.

A cross section (XS1, Fig. 3) was extracted from the LiDAR DEM (Fig. S4B), and at the threshold of overspill of the southern bank (which corresponds to a distance of ~ 25 m on Fig. S4B) was found have an area of 475 m². The water-surface slope during

the flood was assumed to be similar to the regional bedrock slope in the direction parallel to the scour marks ($S = 0.74\%$), which was also extracted from the DEM. These measurements were used, along with a spectrum of roughness-length scales ($0.1 \leq k_s \leq 1$ m) to solve equation (2), resulting in a flow discharge ranging from 800 to 2800 m³/s. Using the same parameters for the incipient-motion calculation above (i.e., $S = 1.85\%$ and $k_s = 0.81$ m), we found that this flood event would have filled the canyon to a depth ranging from 3.7 m to 5.8 m within our measurement reach (Fig. S4C).

Time to excavate the canyon

If sediment transport was the rate limiting step for canyon erosion, a duration of flow needed to carve the canyon can be estimated by dividing the total volume of the canyon (V) by a volumetric transport rate of sediment (Q_s). The total volume of the canyon ($V = 1.53 \times 10^7$ m³) was found using the DEM and differencing a surface interpolated from the topography surrounding the canyon and the topography of the canyon itself. For our estimated range of flood discharge (i.e., 800 - 2800 m³/s) and the corresponding range in hydraulic radii (2.5 – 3.9 m), the volumetric transport rate was calculated as

$$Q_s = 5.7W(rgD_{50}^3)^{1/2} \left(\frac{\tau_b}{r\rho g D_{50}} - \tau_{*c} \right)^{3/2} \quad (3)$$

where $r = (\rho_s - \rho) / \rho = 1.8$ and W is the average bed-width of flow (S8), which at XS2 was found to be 47 m and 56 m for the two discharge estimates (Fig. S4C). This

calculation (i.e., V/Q_s) suggests that flow was sustained for 35 - 160 days to transport the required load out of the canyon.

⁴He Cosmogenic exposure ages

The original up-direction and, if present, original lava-flow surface of the sampled boulders (e.g., Fig. S1B) was identified by basalt density (extent of vesicularity) and vesicle orientation. Samples were taken at least 1-m below volcanic-flow surfaces to avoid inherited exposure that resulted during hiatuses between basalt eruptions. In addition, the sample from the eroded notch was taken from ~2 m below the original flow surface as inferred by tracing bedding surfaces laterally. Helium exposure ages were measured on olivine separates from several kilograms of basalt taken from the upper 4 cm of the exposed surfaces. After extracting any magmatic helium from the olivine, cosmogenic ³He was released from the samples by heating *in vacuo* and measured. Exposure ages were then calculated using an average production rate scaled for latitude, altitude and surface slope. The correction for shielding from canyon walls was found to be less than 4% for all samples and was folded into the error for each age determination. Measurements and calculations are further detailed in (S9).

¹⁴C Radiocarbon ages

The shells were extracted from a ~ 20-cm thick, finely laminated bed containing clay, silt and sand, which is exposed in a small road-cut within the talus slope (Fig. S1C). This bed is probably a backwater deposit from an unknown flood of the Snake River, and appears younger than the Yahoo Clay deposited throughout the region following

damming of the river by McKinny basalt flows (*S10*) ca. 52 ± 24 ka (*S11*), and older than the Bonneville flood (*S12*). Three dates from two shells within the layer yielded ^{14}C radiocarbon ages of 22.51 ± 0.07 ka, 22.55 ± 0.07 ka, and 22.34 ± 0.07 ka. The error bars represent two standard deviations. The first two dates are gas splits from acidification of the same shell. The measurements were made at the Keck Carbon Cycle AMS Facility, Earth System Science Department, University of California -Irvine, U.S.A, following the conventions of (*S13*). Sample preparation backgrounds were subtracted based on measurements of ^{14}C -free calcite.

Supporting Text

Geologic setting

Recently Gillerman et al. (*S14*) reinterpreted the basalt that composes Box Canyon as the Thousand Springs Basalt (also called Basalt of Flat Top Butte; $\sim 395 \pm 20$ ka, (*S11*)), and he inferred the relatively young appearance of bedrock and the origin of Box Canyon to be from scour by the catastrophic Bonneville flood, which drained glacial lake Bonneville ca. 14.5 ka (*S12*). In his autobiography (*S15*), Stearns also admits the possibility that his seepage-erosion hypothesis (*S16*) was incorrect and that the Bonneville flood carved Box Canyon and scoured the neighboring landscape. Hydraulic modeling by O'Conner (*S17*), however, showed that the Bonneville flood did not overflow the Snake River Canyon in this region, which is consistent with our dating and analysis that Box Canyon was carved by an older event(s). U-Th/He eruption ages (*S9*) confirm that the basalt of Box Canyon is 86 ± 12 ka to 130 ± 12 ka and this is consistent

with the earlier designation of Sand Springs Basalt (*S18, S19*) (also named the Basalt of Rocky Butte (*S14*)) with an Ar-Ar eruption age of $\sim 95 \pm 10$ ka (*S11*).

Near the mouth of Box Canyon, the Quaternary basalt overlies a ~ 5 -m thick Pliocene or Miocene stratified volcanoclastic unit (*S14, S20*), which appears older and more weathered than the basalt. This unit is only exposed near the canyon mouth, where the talus slope was excavated recently for an aqueduct. Most of the canyon floor is composed of basalt boulders so the underlying bedrock cannot be determined.

Quaternary basalt is exposed, however, at a ~ 5 -m high waterfall (Fig. S5A) approximately 730 m downstream of the canyon head (Figs. 3 and S3). The log from the nearest well, about 0.5 km southeast of the canyon head, extends to a depth of 43 meters, or ~ 7 m below the canyon floor near the headwall, and indicates intact basalt to this depth (*S21*). Thus, if the underlying older unit is laterally extensive, it does not appear to have played a role in formation of the canyon, at least upstream of the waterfall.

Spring discharge and chemistry

Fig. S6 shows the daily average discharge and the dissolved silica concentration for Box Canyon creek as recorded by the U.S. Geological Survey (*S7*). The saturation value of 33 mg/L was calculated for dissolved quartz and amorphous silica at 14° C and pH = 8 (*S22*), conditions typical of Box Canyon creek. Seasonal variations in discharge are less than 10 to 20% and trends over the 58-year duration of record are thought to record changes in farm irrigation across the plain, rather than natural forcing.

Talus at the canyon head

It is puzzling that there is almost no talus at the canyon head (Fig. S5B), while talus slopes are well developed elsewhere in the canyon. Our date of the notch at the canyon head suggests that wall collapse has not occurred there since ca. 45 ka. Perhaps, the basalt columns are more interlocked at the headwall, which might also explain why the headwall stalled at this location during canyon formation. Alternatively, maybe the spring flow prevents rock breakdown at the headwall, e.g. by preventing freeze-thaw (S23).

Delta at the canyon mouth

There appears to be a small delta ($\ll 1\%$ of the total canyon volume) at the mouth of Box Canyon (Fig. S5C). This might imply that there has been active transport of sediment since ca. 14.5 ka when the Bonneville flood swept through the Snake River Canyon (S17), or perhaps sediment transport occurred within Box Canyon because of withdrawal of the Bonneville floodwater.

Bedrock scour directions

Bedrock scours near the canyon head indicate flow towards the canyon headwall (Fig. 3). We identified three locations near the canyon mouth, however, with bedrock scours that appear to display an opposite flow direction with orientations ranging from 113° to 115° (Table S1). The consistency of these directions, all aligned with the prevailing westerly wind direction, suggests that these outliers resulted from wind abrasion. A high knob of bedrock ~ 7.8 km to the east of Box Canyon also shows scours orientated 110° consistent with this hypothesis.

Supporting Figures



Fig. S1. (A) Photograph of the measurement reach and cross section XS2 within Box Canyon (the stream is ~ 35 m wide for scale). (B) Photograph of the boulder at location 2 (Fig. 3) sampled for ^4He cosmogenic exposure dating. (C) Photograph of a sediment deposit exposed within the talus slope (location 5, Fig. 3) containing shell fragments that were used for ^{14}C dating.

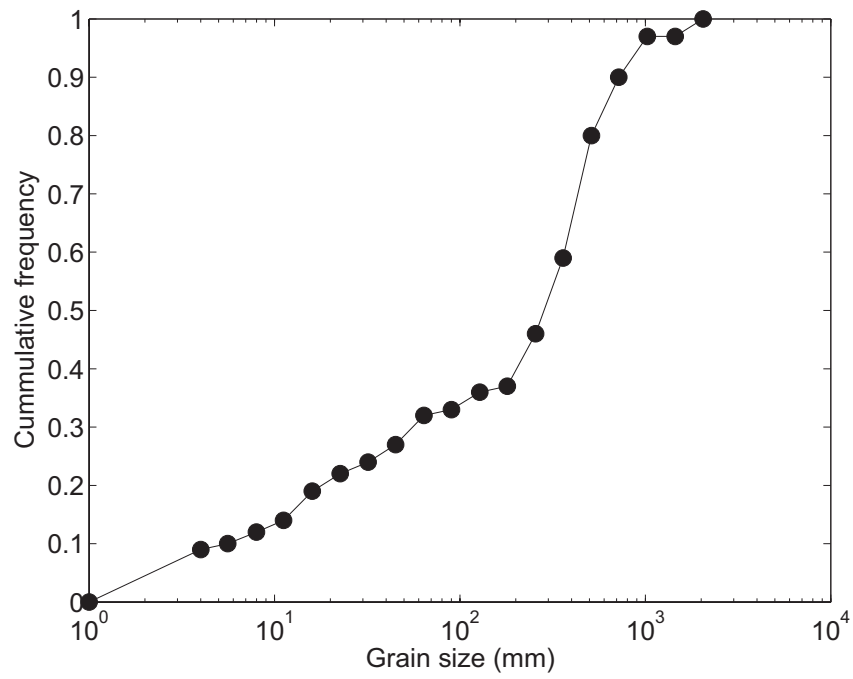


Fig. S2. Cumulative frequency distribution of particle sizes along the stream bed of Box Canyon within the measurement reach.

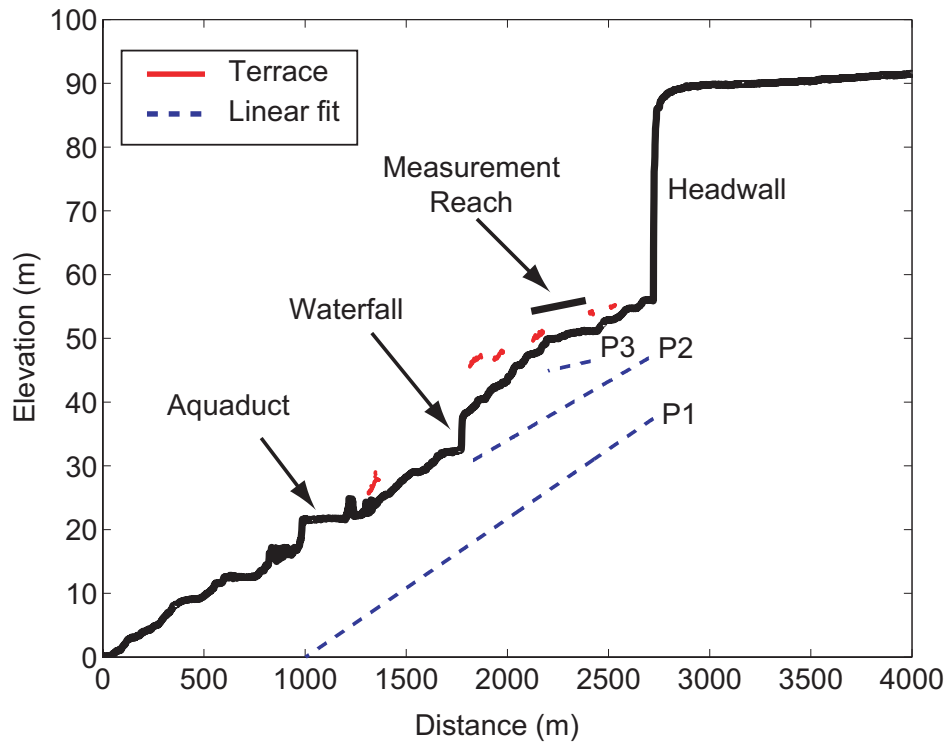


Fig. S3. Longitudinal profile of Box Canyon calculated as the path of steepest descent from the 1-m resolution DEM. Three linear, least-squares fits to the data, used to calculate channel-bed slope, are shown as dashed lines (displayed offset from the data) for P1: the entire length of the canyon ($S = 2.18\%$), P2: a 900-m reach bounded by the waterfall and the canyon head ($S = 1.85\%$), and P3: the measurement reach ($S = 0.9\%$). The elevations of mapped terraces (Fig. 3) are shown in red.

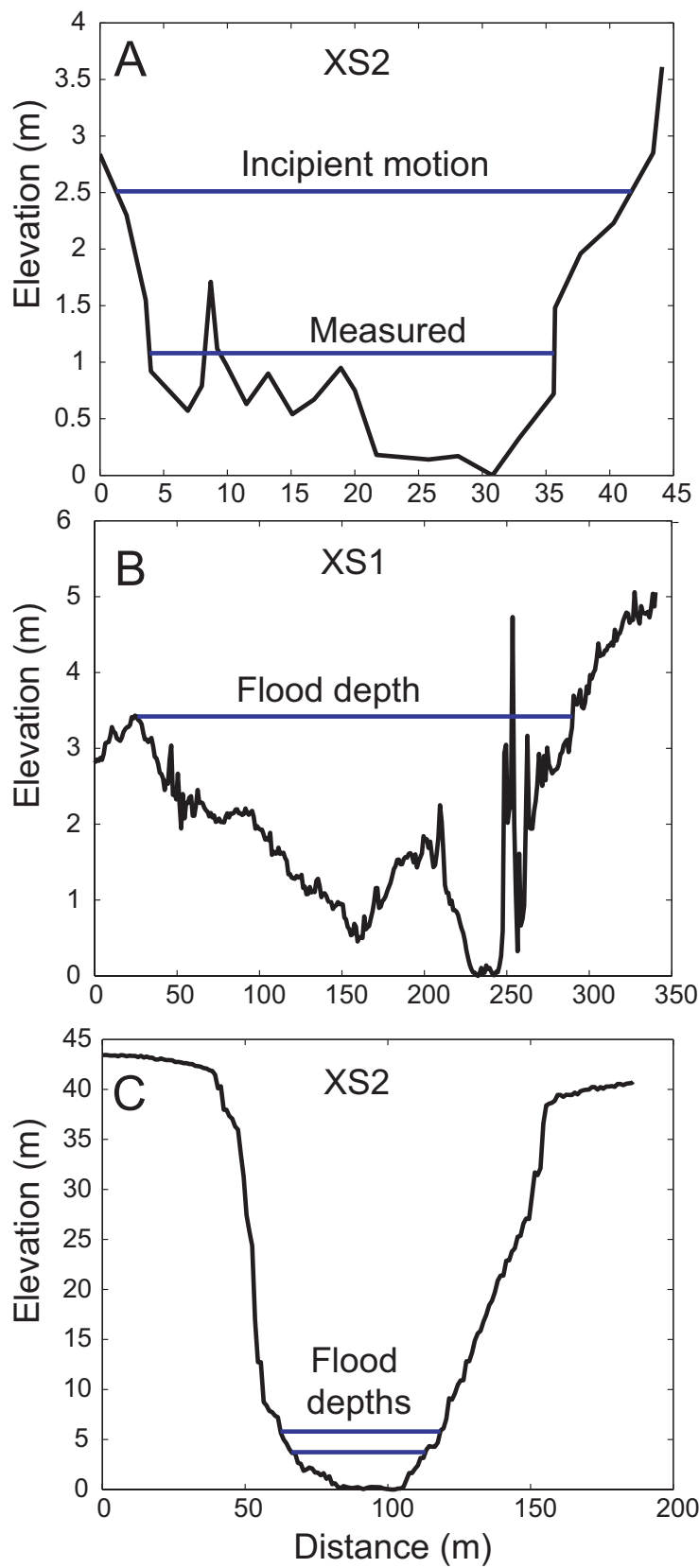


Fig. S4. Cross sections of Box Canyon. (A) XS2 (Fig. 3) along the stream bed showing the bed and water surface topography surveyed in the field, as well as the calculated depth for incipient motion. (B) XS1 (Fig. 3) extracted from the DEM showing the depth used to constrain the flood discharge. (C) XS2 extracted from the DEM showing a range in depths that correspond to the range in calculated flood discharges.



Fig. S5. Photographs of Box Canyon showing the (A) ~ 5-m high waterfall, (B) ~ 35-m high canyon headwall, and (C) small delta at the confluence with the Snake River (the Snake River is ~ 200 m wide for scale).

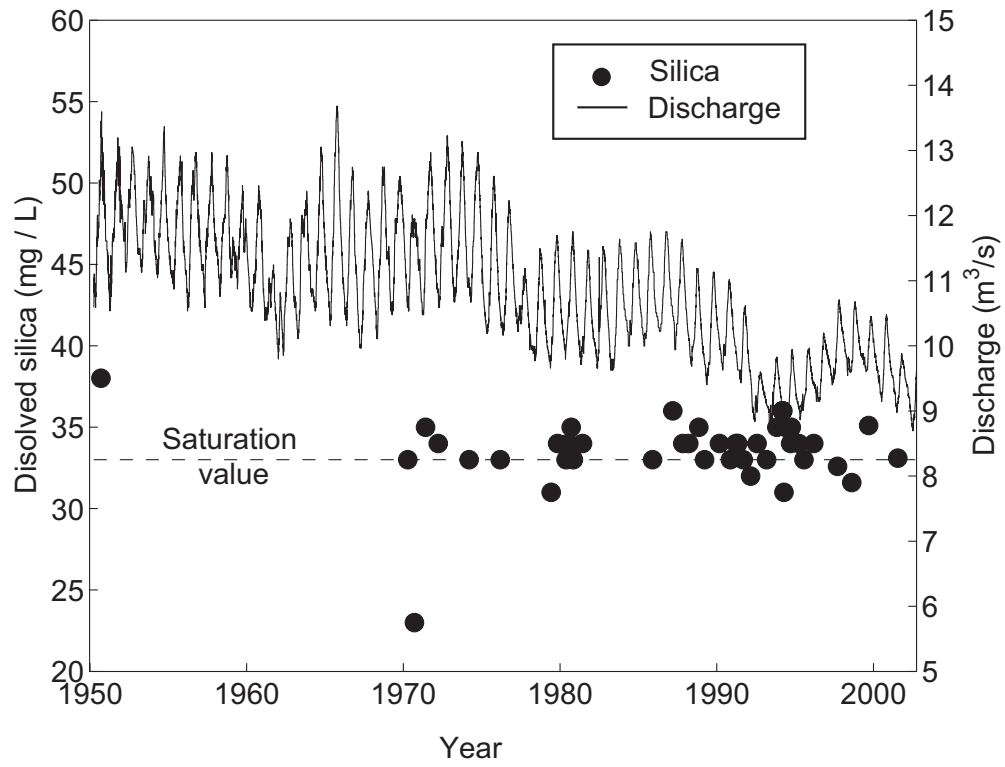


Fig. S6. Discharge and dissolved silica records for Box Canyon creek from the U.S. Geological Survey gauge 13095500.

Supporting Tables

Table S1 – Inferred wind abrasion marks.

| Location | Longitude | Latitude | Scour orientation |
|-----------------|------------------|-----------------|--------------------------|
| Box Canyon | 42.70566° | -114.81971° | 113° |
| Box Canyon | 42.70902° | -114.81895° | 115° |
| Box Canyon | 42.70874° | -114.82214° | 115° |
| 7.8 km East | 42.7163° | -114.70708° | 110° |

Supporting References and Notes

- S1. A. Shields, *Mitt. Preuss. Versuchsanst. Wasserbau Schiffbau* **26**, 26 (1936).
- S2. J. M. Buffington, D. R. Montgomery, *Water Resources Research* **33**, 1993 (1997).
- S3. D. R. Montgomery, J. M. Buffington, *Geological Society of America Bulletin* **109**, 596 (1997).
- S4. M. P. Lamb, W. E. Dietrich, J. Venditti, *Journal of Geophysical Research* in press, (available at <http://www.agu.org/journals/pip/jf/2007JF000831-pip.pdf>).
- S5. J. C. Bathurst, *Journal of Hydrology* **269**, 11 (2002).
- S6. J. W. Kamphuis, *Journal of Hydraulic Research* **12**, 193 (1974).
- S7. U.S. Geological Survey, gauge 13095500, Box Canyon Creek, Idaho
- S8. R. Fernandez Luque, R. van Beek, *J. Hydraul. Res.* **14**, 127 (1976).
- S9. S. M. Aciego *et al.*, *Earth and Planetary Science Letters* **254**, 288, doi:10.1016/j.epsl.2006.11.039 (2007).
- S10. H. E. Malde, in *Cenozoic Geology of Idaho* B. Bonnicksen, R. M. Breckenridge, Eds. (1982), vol. 26, pp. 617-628.
- S11. L. Tauxe, C. Luskin, P. Selkin, P. Gans, A. Calvert, *Geochemistry Geophysics Geosystems* **5**, doi:10.1029/2003GC000661 (2004).
- S12. W. E. Scott, K. L. Pierce, J. P. Bradbury, R. M. Forester, in *Cenozoic Geology of Idaho: Idaho Bureau of Mines and Geology Bulletin* G. Bonnicksen, R. M. Breckenridge, Eds. (1982), vol. 26, pp. 581-595.
- S13. M. Stuiver, H. A. Polach, *Radiocarbon* **19**, 355 (1977).

- S14. V. S. Gillerman, J. D. Kauffman, K. L. Otherberg, *Geologic map of the Thousand Springs Quadrangle, Gooding and Twin Falls counties, Idaho* (Idaho Geological Survey, Moscow, Idaho, 2004).
- S15. H. T. Stearns, *Journal of Geology* **44**, 429 (1936).
- S16. H. T. Stearns, *Memoirs of a Geologist: From Poverty Peak to Piggery Gulch* (Hawaii Institute of Geophysics, Honolulu, Hawaii, 1983).
- S17. J. E. O'Connor, *Hydrology, Hydraulics and Geomorphology of the Bonneville Flood*, GSA Special Paper 274 (Geological Society of America, Boulder, CO, 1993), pp. 90.
- S18. H. E. Malde, *U.S. Geological Survey Professional Paper*, 20 (1971).
- S19. H. R. Covington, J. N. Weaver, *Geologic map and profiles of the north wall of the Snake River Canyon, Thousand Springs and Niagara Springs quadrangles, Idaho*, U.S. Geological Survey Miscellaneous Investigations I-1947C (1991).
- S20. H. E. Malde, H. A. Powers, *Geological Society of America Bulletin* **73**, 1197 (1962).
- S21. Elsing Well Drilling, Well Log # 40916, Department of Water Resources, Idaho (1975).
- S22. G. Faure, *Principles and Applications of Geochemistry* (Prentice Hall, Upper Sadle River, ed. 2nd, 1998), pp. 600.
- S23. L. J. Mason, D. T. Pederson, R. J. Goble, *Eos Trans. AGU Fall Meet. Suppl.* **85**, Abstract H51C (2004).